ADVANCES IN ATMOSPHERIC SCIENCES, VOL. 24, NO. 4, 2007, 712–728

Performance of a Reconfigured Atmospheric General Circulation Model at Low Resolution

WEN Xinyu*[1] (闻新宇), ZHOU Tianjun[2] (周天军), WANG Shaowu (王绍武), WANG Bin (王 斌), WAN Hui (万 慧), and LI Jian (李 建)

[1]*Department of Atmospheric Sciences, School of Physics, Peking University, Beijing* 100871

[2]*State Key Laboratory of Numerical Modeling for Atmospheric Sciences and Geophysical Fluid Dynamics, Institute of Atmospheric Physics, Chinese Academy of Sciences, Beijing* 100029

(Received 14 January 2006; revised 1 June 2006)

ABSTRACT

Paleoclimate simulations usually require model runs over a very long time. The fast integration version of a state-of-the-art general circulation model (GCM), which shares the same physical and dynamical processes but with reduced horizontal resolution and increased time step, is usually developed. In this study, we configure a fast version of an atmospheric GCM (AGCM), the Grid Atmospheric Model of IAP/LASG (Institute of Atmospheric Physics/State Key Laboratory of Numerical Modeling for Atmospheric Sciences and Geophysical Fluid Dynamics), at low resolution (GAMIL-L, hereafter), and compare the simulation results with the NCEP/NCAR reanalysis and other data to examine its performance. GAMIL-L, which is derived from the original GAMIL, is a finite difference AGCM with 72×40 grids in longitude and latitude and 26 vertical levels. To validate the simulated climatology and variability, two runs were achieved. One was a 60-year control run with fixed climatological monthly sea surface temperature (SST) forcing, and the other was a 50-yr (1950–2000) integration with observational time-varying monthly SST forcing. Comparisons between these two cases and the reanalysis, including intra-seasonal and inter-annual variability are also presented. In addition, the differences between GAMIL-L and the original version of GAMIL are also investigated.

The results show that GAMIL-L can capture most of the large-scale dynamical features of the atmosphere, especially in the tropics and mid latitudes, although a few deficiencies exist, such as the underestimated Hadley cell and thereby the weak strength of the Asia summer monsoon. However, the simulated mean states over high latitudes, especially over the polar regions, are not acceptable. Apart from dynamics, the thermodynamic features mainly depend upon the physical parameterization schemes. Since the physical package of GAMIL-L is exactly the same as the original high-resolution version of GAMIL, in which the NCAR Community Atmosphere Model (CAM2) physical package was used, there are only small differences between them in the precipitation and temperature fields. Because our goal is to develop a fast-running AGCM and employ it in the coupled climate system model of IAP/LASG for paleoclimate studies such as ENSO and Australia-Asia monsoon, particular attention has been paid to the model performances in the tropics. More model validations, such as those ran for the Southern Oscillation and South Asia monsoon, indicate that GAMIL-L is reasonably competent and valuable in this regard.

Key words: GCM, GAMIL-L, atmosphere, model validation

DOI: 10.1007/s00376-007-0712-7

1. Introduction

State-of-the-art coupled climate system models are the best tool for making simulations of past and future climate changes because of their comprehensive representation of the climate system. However, some applications of these models are limited by their expensive computation costs. For example, paleoclimate simulations usually require large amounts of computer time and storage space, especially when different climatolo-

*Corresponding author: WEN Xinyu, xywen@pku.edu.cn

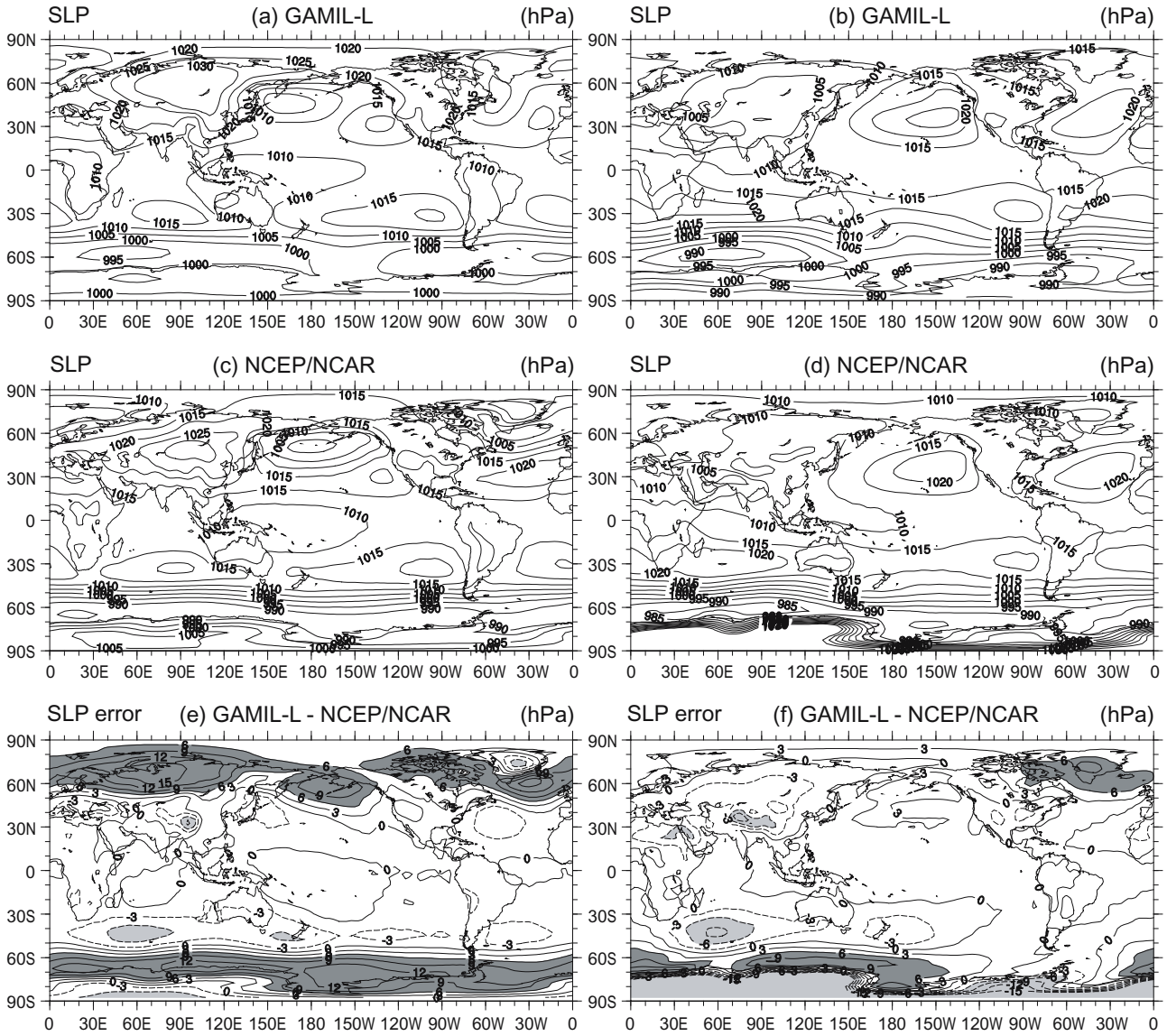

Fig. 1. Mean sea level pressure (hPa) for DJF (left) and JJA (right) from the model (top row) and the NCEP/NCAR reanalysis (middle row) and the model minus reanalysis differences (bottom row). The contour increment in the top 2 rows is 5 hPa. Differences are contoured every 3 hPa from 0 hPa, and positive (negative) differences that are statistically significant at the 95% level for a t-test are shaded in dark gray (light gray).

gical backgrounds or scenarios are being considered. For ocean-atmosphere coupled models, it usually takes hundreds of years for the oceanic component to reach equilibrium. One example is the Permian simulation with NCAR Community Climate System Model (CCSM3). This coupled simulation has taken 2000 model years to spin up the oceanic component, which is one of the most computationally expensive experiment carried out on NCAR supercomputers (Climate and Global Dynamics Division, 2004). At present, this kind of long-term coupled climate simulation remains a great computational challenge for the climate modeling community. Thus, how to shorten the spin-up process under present computer abilities is a crucial open question. Generally, two common approaches are taken to solve this problem: modifying the coupling schemes, or reducing the resolution of the atmosphere and/or ocean component models (Liu et al., 2004). However, in addition to these two methods, another study attempted to use a more complicated technique—deep ocean acceleration technique—to solve the problem (Boville and Gent, 1998).

To modify the coupling schemes, two kinds of acceleration schemes have usually been used over the past few decades: asynchronous coupling and periodically synchronous coupling (Liu et al., 2004). However, due

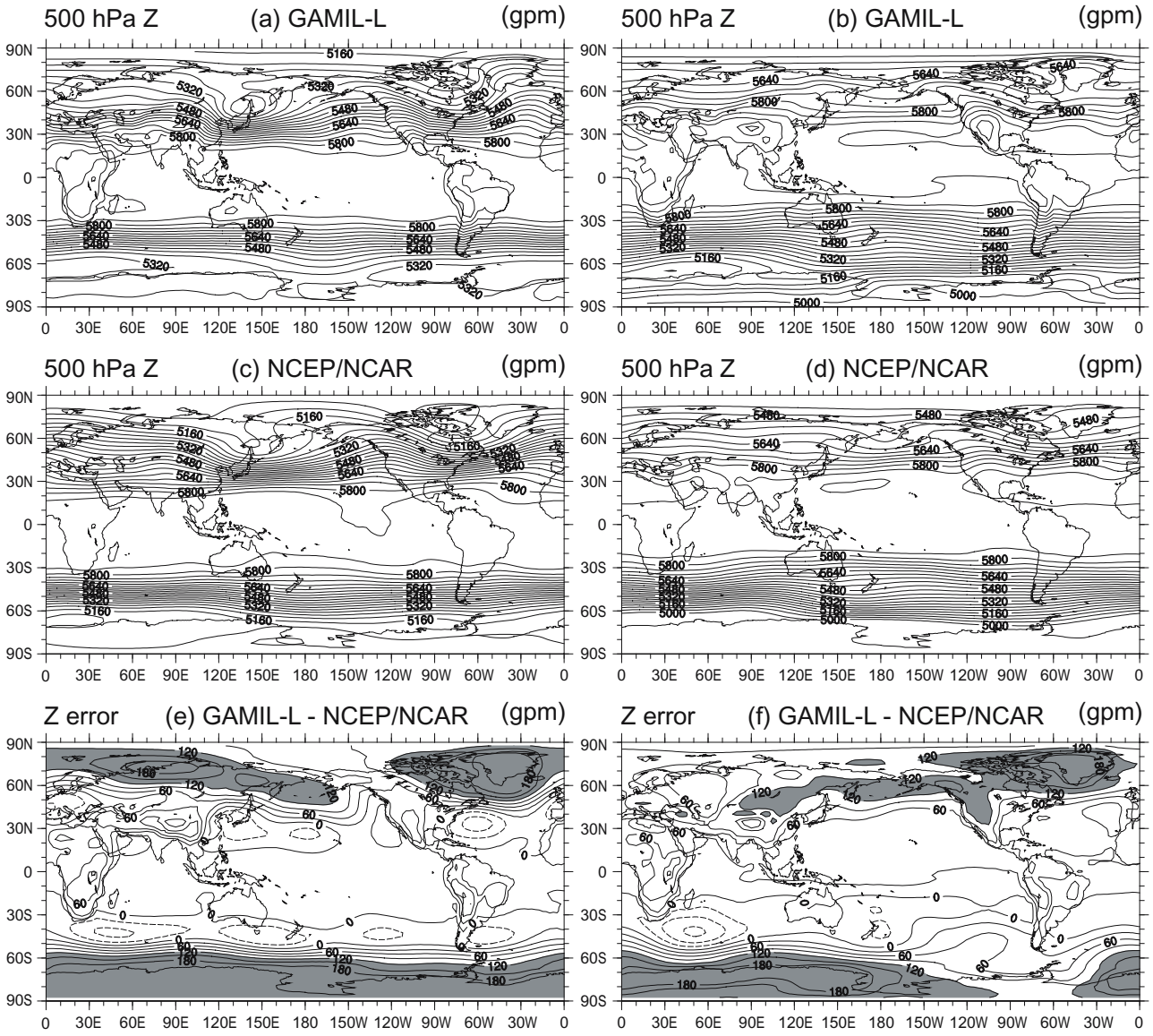

Fig. 2. Same as Fig. 1, but for mean 500 hPa geopotential height (gpm). The contour increment in the top two rows is 40 gpm. Differences are contoured every 30 gpm from 0 gpm.

to their complexity, they have not been widely used.

Another way to accelerate model integrations is to simply reduce the model resolution of the atmospheric and/or oceanic component models, especially for the atmospheric component. It is known that in a coupled GCM, the atmospheric component generally plays a predominant role in both running speed and storage space because of its complicated radiation transfer schemes and hydrological treatments. Hence, one common approach is to reduce the resolution of the atmospheric model in order to accelerate the integration. FOAM (Fast Ocean-Atmosphere Model) is a good example (Jacob et al., 2001; Tobis et al., 1997). Its atmospheric component comes from a parallel version of NCAR Community Climate Model (CCM2), but on an R15 grid (40×48 in latitude and longitude). Although it has the weakness of coarse resolution, its capability at capturing many of the climatological features is good. At present, FOAM is one of the fastest coupled atmospheric-oceanic GCMs (AOGCM). It can integrate for 8–38 years on various platforms per day, and so can be used for a great many paleoclimate studies. Similarly fast versions of coupled climate models have been developed in many climate modeling centers, such as the Goddard Institute for Space Studies (Russell et al., 1995), the Geophysical Fluid Dynamics Laboratory (GFDL) (Dixon et al., 2003), the National Center for Atmospheric Research Community Climate

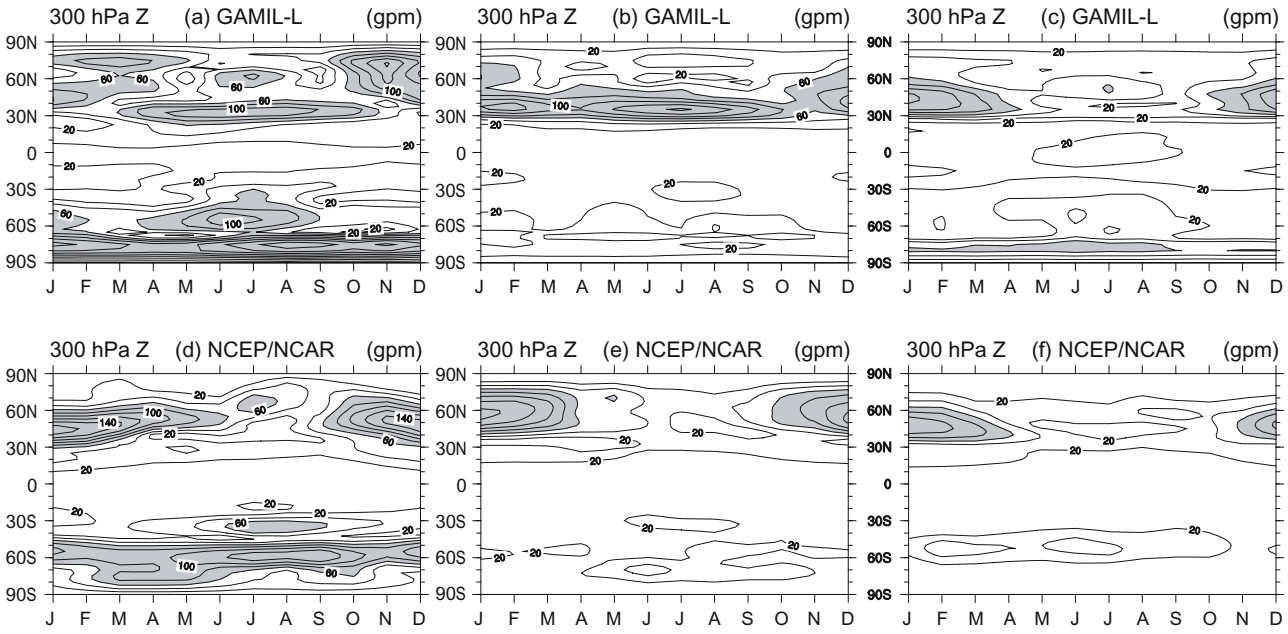

Fig. 3. Annual march of the amplitude of wave number 1 (left), 2 (center) and 3 (right) at 300 hPa from the model (top row) and the NCEP/NCAR reanalysis (bottom row). The contour increment in all panels is 20 gpm. Amplitude greater than 60 gpm are shaded in light gray.

System Model (Blackmon et al., 2001), and the Hadley Centre (Jones et al., 2005).

In order to develop a fast version of the coupled climate system model suitable for paleoclimate studies, especially for the simulations that need integrations over an extremely long period, collaborating with the Department of Atmospheric Sciences of Peking University (PKU), IAP/LASG has devoted great effort to the development of a new fast version of the atmospheric component model, viz. GAMIL-L, which is configured based on the original Grid Atmosphere Model of IAP/LASG (GAMIL) (Wang et al., 2004).

In this study, we validate the climatological mean state and the inter-annual variability simulated by GAMIL-L, to ensure its performance in a fully coupled GCM. The paper is organized as follows: a brief description of GAMIL-L and validation datasets is presented in section 2; differences between simulations and the reanalysis are described and analyzed in section 3; changes to the original version of GAMIL, especially over the polar regions, are examined in section 4; and a brief conclusion of the model's performance, both in terms of its successes and failings, is drawn in the final section.

2. Model, experiments and validation data

IAP/LASG has developed a number of AGCMs during recent decades (Zeng et al., 1987; Zhang et al., 1992; Wu et al., 1996, 2003; Wang et al., 2004; Bao et al., 2005). Up to now, two series AGCMs, grid models and spectral models, have been established successfully. The original GAMIL is a global grid atmospheric model, with a horizontal grid size of approximately 2.8°(lon)×3°(lat), equal-area mesh, 26 vertical levels in a sigma coordinate, and a top level at 2.194 hPa. The physics package used in GAMIL is derived from NCAR CAM2 and CCM3 (Hack et al., 1998; Hurrell et al., 1998; Kiehl et al., 1998a,b). A complete description of the dynamical framework and numerical methods used in GAMIL is provided by Wang et al. (2004).

The development of GAMIL-L was motivated by the need of paleoclimate simulations, and its parameters are as follows: GAMIL-L uses a 72×40 weighted equal-area mesh, which corresponds to approximately a 5° (lon)×4.5° (lat) grid. Consequently, apart from the two polar regions, both the tropical and mid latitude regions can be resolved well. Meanwhile, the new time step for dynamical core integration is set to five minutes, while the new time step for physical processes integration is half an hour. These time steps are considerably longer than in the original GAMIL settings (120 seconds for dynamics and 20 minutes for physics), and as a result, GAMIL-L integrates four times faster than the original GAMIL.

Two sets of experiments were carried out with GAMIL-L: one was a control run of 60 years with prescribed climatological SST forcing, and the second was a 50-year integration forced with the obser-

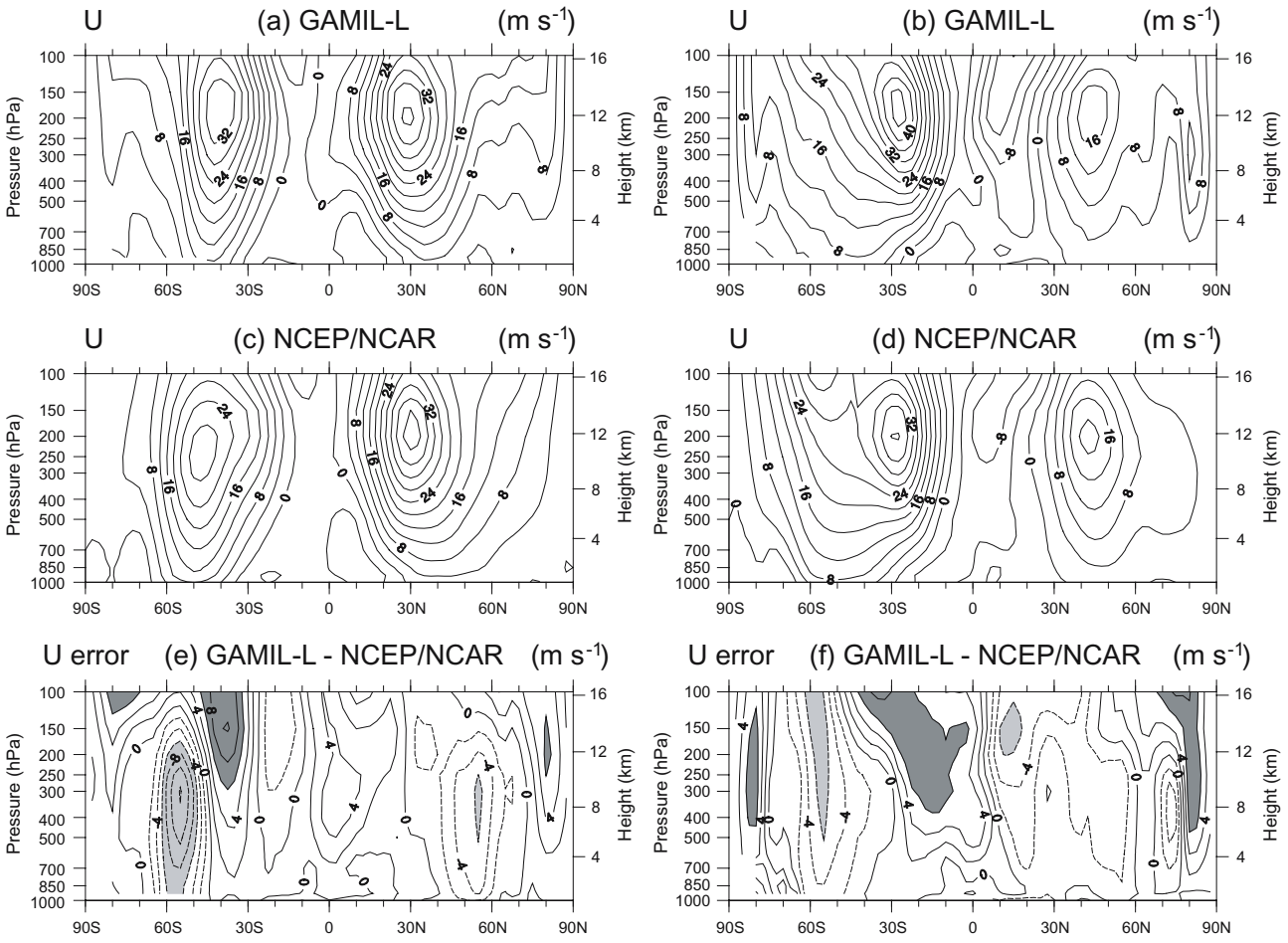

Fig. 4. Same as Fig. 1, but for mean zonally-averaged zonal wind (m s^{-1}). The contour increment in the top two rows is 4 m s^{-1}. Differences are contoured every 2 m s^{-1} from 0 m s^{-1}, and positive (negative) differences that are statistically significant at the 95% level for a t-test are shaded in dark gray (light gray).

vational monthly SST from 1945–2000 (Rayner et al., 2003). The control run was used to validate the climatological mean state, and the second integration was used to examine the inter-annual variability simulated by GAMIL-L. In order to compare the differences between GAMIL-L and its original version, a 30-year run of GAMIL with prescribed climatological SST focing was completed.

The National Centers for Environmental Prediction and National Center for Atmospheric Research (NCEP/NCAR) reanalysis dataset (referred to as NCEP reanalysis) was used to evaluate the simulated climatology (Kalnay et al., 1996). The archive used here consists of 50 years (1951–2000) of monthly data, which were interpolated from 2.5° × 2.5° grid to the GAMIL-L grid for comparison. In addition, the observational precipitation were taken from NCEP CPC (Climate Prediction Center) Merged Analysis of Precipitation (CMAP), which is a version of analyses of global precipitation using gauge observations, satellite estimates, and numerical model predictions (Xie and Arkin, 1996). The CMAP data over 1981–2000 were averaged to give an appropriate estimate of climatological precipitation fields.

3. Results

3.1 *Sea level pressure*

The mean sea level pressure (SLP) pattern is a useful indication of an AGCM's ability to simulate the atmospheric circulation near the surface, and it represents an integrated measure of a model's thermodynamic and dynamic representations. The model produces the basic characteristics of observed mean SLP distribution in the tropics and mid latitudes (Fig. 1). However, the biases over high latitudes of both hemispheres are large. During boreal winter (December-January-February, DJF hereafter), the arctic vortex simulation is poor, with an unrealistic high center over this area. Also, the Southern Hemisphere storm track

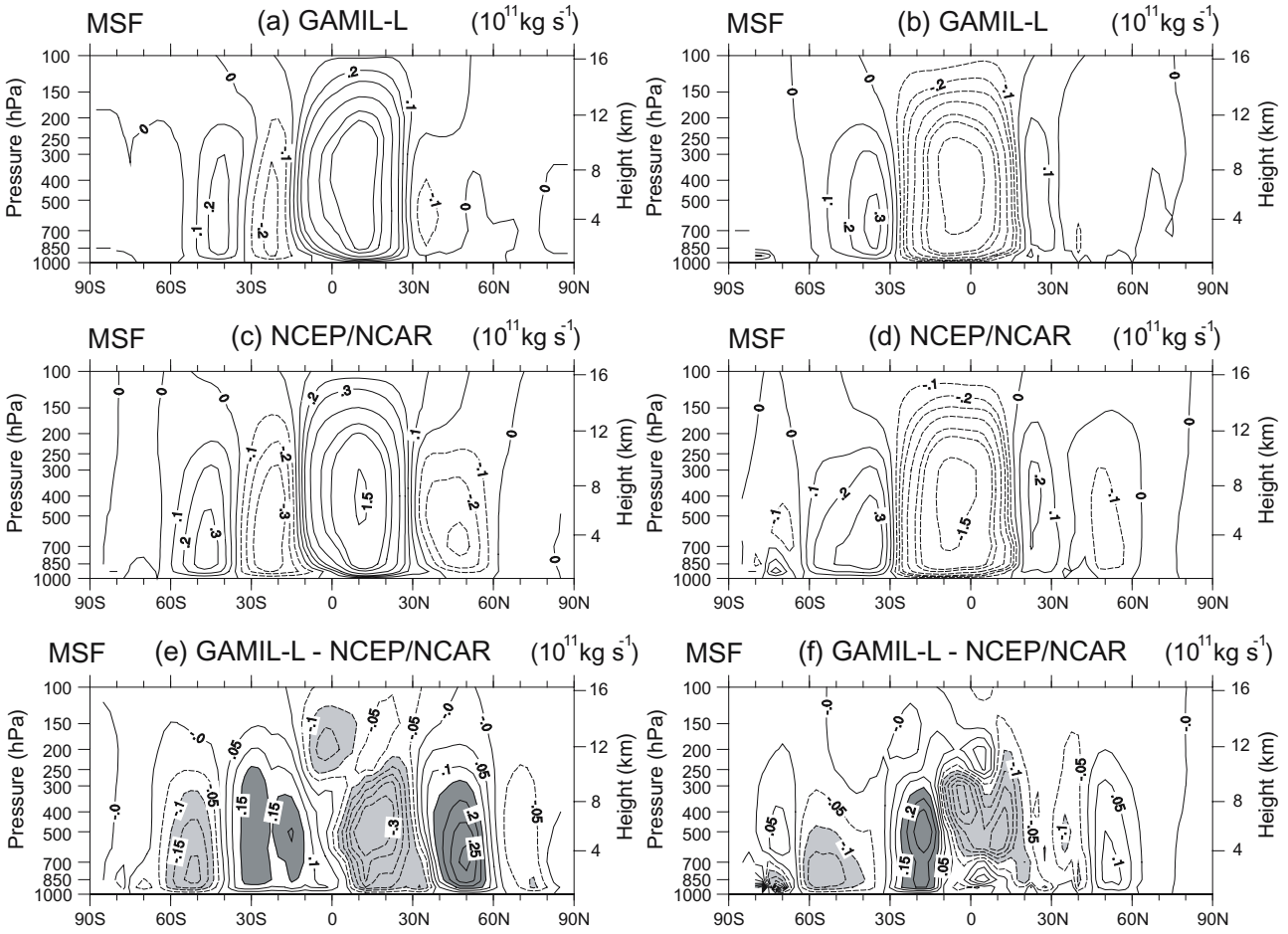

Fig. 5. Same as Fig. 1, but for mean meridonal stream function ($\times 10^{11}$ kg s^{-1}). The contour in the top two rows is plotted in nonlinear levels (± 0.1, ± 0.2, ± 0.3, ± 0.5, ± 0.8, ± 1.0, ± 1.5, $\pm 2.0 \times 10^{11}$ kg s^{-1}). Differences are contoured every 0.05×10^{11} kg s^{-1} from 0 kg s^{-1}.

(50°–80°S) is not simulated well. The higher sea level pressure (SLP) in the model over this region means less eddy activities than in reality. During boreal summer (June-July-August, JJA hereafter), notable errors appear over the Antarctica continent (Fig. 1f), although there are large uncertainties in the NCEP/NCAR reanalysis over this area due to the dearth of observations. Apart from high latitudes, for both DJF and JJA, GAMIL-L captures the broad SLP patterns over tropical and extra-tropical areas, although substantial differences exist over the North Pacific, Eurasia and other regions. In particular, the simulated subtropical highs are slightly weaker than those in the reanalysis. Consequently, they will correspond to two weak Hadley cell branches.

During DJF, the simulated SLP is characterized by a weaker Aleutian low, weaker Icelandic low, stronger Siberian high, weaker subtropical high zones, and a weaker Antarctica circumpolar low. Similarly, during JJA, it is mainly characterized by a weaker Mascarene high and a stronger Indian low. In particular, over the East Asian summer monsoon area, we can see a slightly stronger Pacific high corresponding to a stronger continental low.

3.2 *Geopotential height*

The pattern of the 500 hPa geopotential height field (Fig. 2) is a good representative of the mid-tropospheric atmospheric circulation. During DJF, the positions of the major troughs and ridges over northern high latitudes simulated by GAMIL-L are qualitatively consistent with the reanalysis. During JJA, GAMIL-L also successfully reproduces the observed large-scale zonal symmetries of the 500 hPa geopotential height, and the northern subtropical high over the Pacific and Atlantic, but produces two unrealistic closed high centers over the Himalayas and the Rocky Mountain. Over almost all high latitudes, the simulated values are higher than the NCEP reanalysis. The bias in the geopotential height is related to the un-

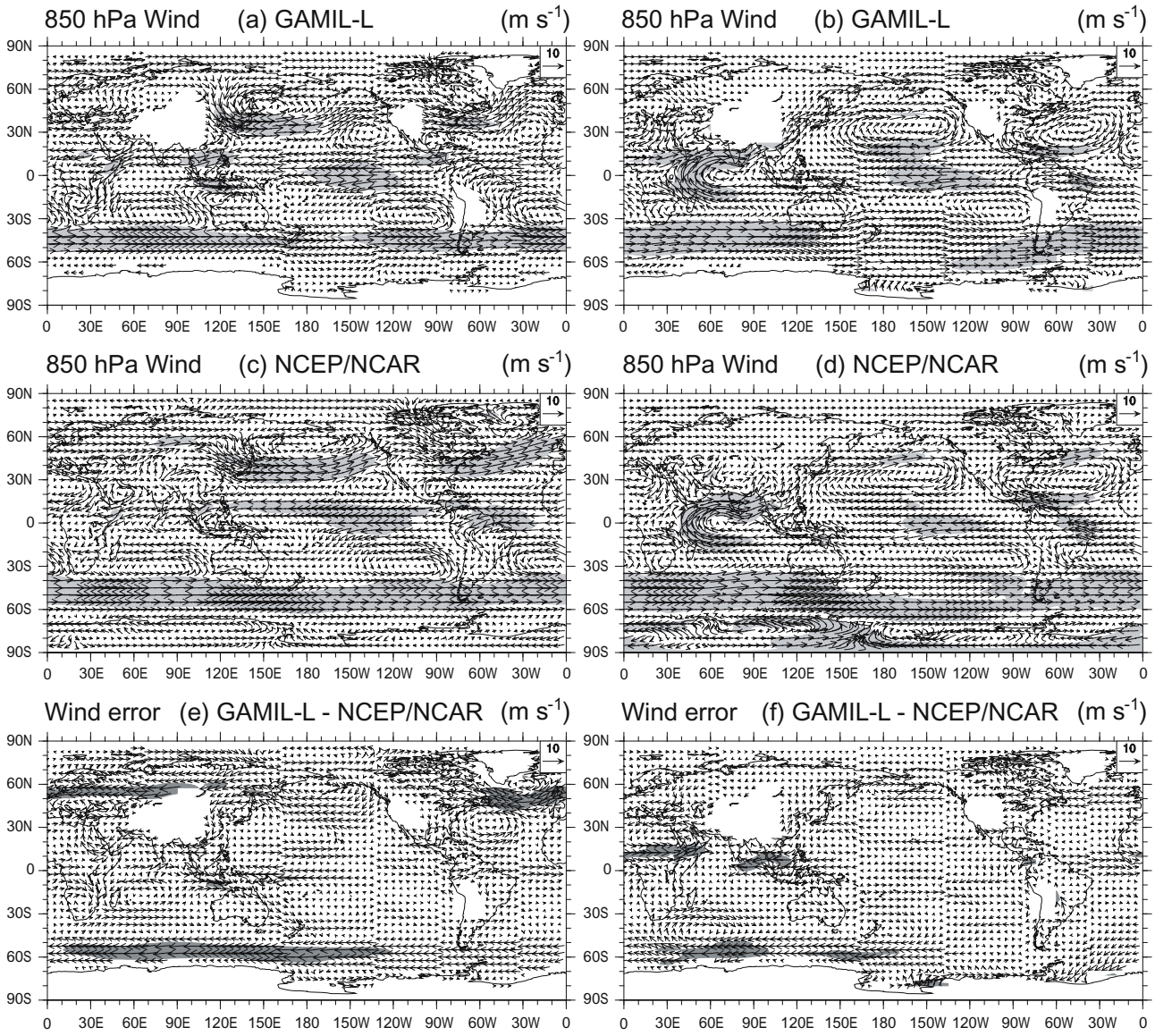

Fig. 6. Same as Fig. 1, but for mean wind vector (m s^{-1}) at 850 hPa. The values of wind velocity greater than 5 m s^{-1} are shaded in light gray in the top two rows.

realistic simulation of the structure of the tropospheric temperature, especially in the lower troposphere over high latitudes, which will be discussed below. Because of the warm biases in the simulated temperature, the meridional gradient of 500 hPa geopotential height becomes weaker than the reanalysis.

Large-scale deviations from zonal means are described well by a Fourier decomposition of the geopotential heights along latitude circles. Raphael (1998) provided a detailed analysis of the Southern Hemisphere (SH) quasi-stationary waves in the CCM3 during DJF and JJA. Using this method, the annual cycles of the amplitudes of wave numbers 1–3 at 300 hPa are presented in Fig. 3 for both GAMIL-L and the NCEP reanalysis. According to the theory of wave decomposition, wave number 1 represents the position of the polar vortex; wave number 2 can be considered as the stationary wave due to positions of continents and oceans; and wave number 3 likens the observations relatively. Together, wave numbers 1–3 are so-called quasi-stationary waves. For wave number 1, GAMIL-L captures the major seasonal and latitudiual variations seen in the reanalysis, but one unrealistic high center exists between 20°–40°N during JJA. For wave number 2, GAMIL-L also overestimates one large amplitude center between 30°–60°N during JJA. The simulation for wave number 3 is very acceptable. The biases in wave numbers 1–2 may be related to the coarse reso-

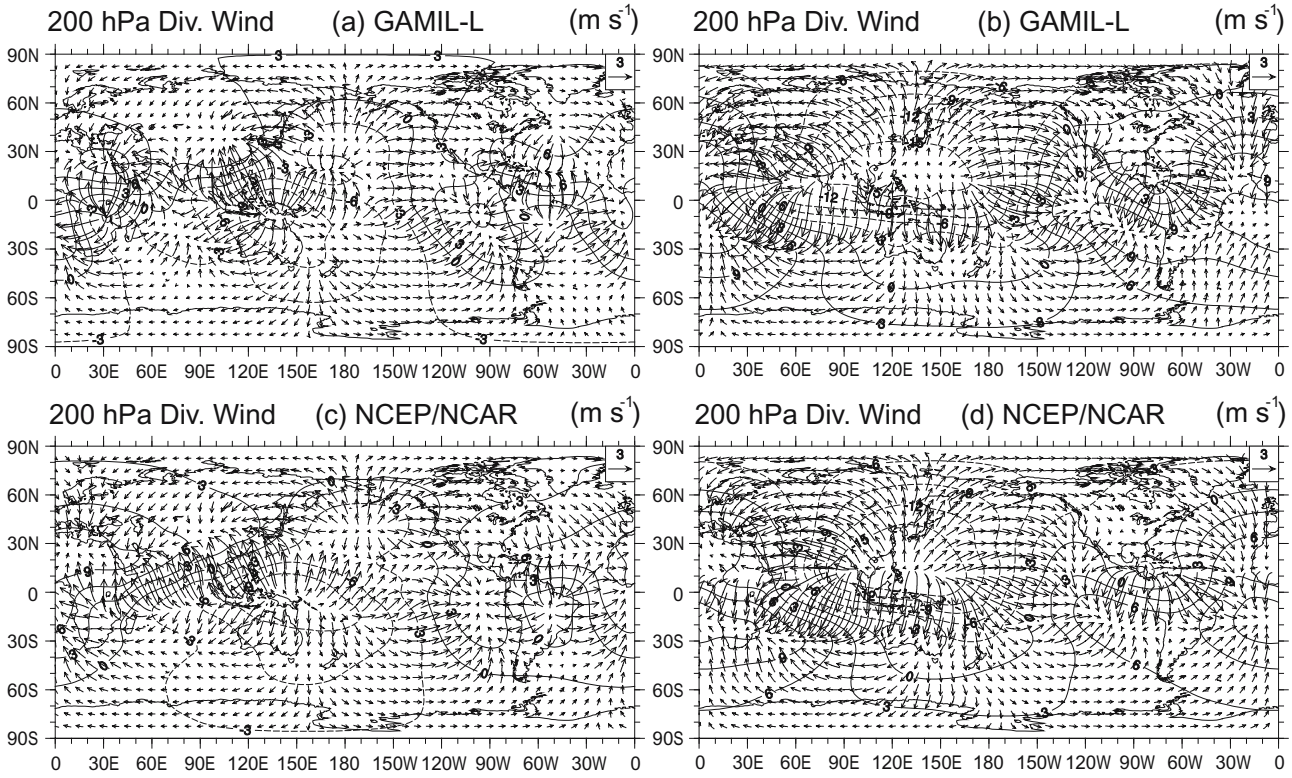

Fig. 7. Mean velocity potential ($\times 10^6$ m^2 s^{-1}) and vector divergent wind (m s^{-1}) at 200 hPa for DJF (left) and JJA (right) from the model (top row) and the NCEP/NCAR reanalysis (bottom row). The contour increment of velocity potential in all panels is 3×10^6 m^2 s^{-1}.

lution of GAMIL-L.

Overall, the large-scale features of the atmospheric circulation is reasonably simulated by GAMIL-L, although large regional biases exist. It implies that the dynamical characteristic of this model is acceptable, especially over the tropics and mid latitudes.

3.3 *Winds*

Figure 4 compares the simulated and the reanalysis zonal mean wind component (U). In the troposphere, the observed zonal mean wind is characterized by two subtropical jet cores near 30° of the winter hemisphere and near 40° of the summer hemisphere, with the strongest westerlies of 40 m s^{-1} at the 200 hPa level (Fig. 4c). This large-scale pattern is well simulated by GAMIL-L. The strength of the simulated jet cores is, however, always stronger than in the reanalysis, while the strength of Northern Hemisphere (NH) jet cores is weaker than the reanalysis. Both of these biases are due to the unrealistic simulation of the temperature structure above 300 hPa in the upper troposphere (Fig. 8), with too strong a meridional temperature gradient leading to much stronger zonal wind.

The meridional circulation in the tropics reflects atmospheric response to direct thermodynamic forcing. The zonal mean meridional stream function simulated by GAMIL-L (Fig. 5) shows that, during DJF, both the Hadley and Ferrell cells are consistently weaker than in the reanalysis. During JJA, the meridional cells are also simulated weakly. It implies that less energy and water vapor are transported from the summer hemisphere to the winter hemisphere. These results imply weak convection within the ITCZ in GAMIL-L, as shown below.

Figure 6 shows that the major features of the 850 hPa wind are captured by GAMIL-L. During DJF, the model simulates the westerly maxima off the east coasts of Asia and North America, where the storm tracks are located, although they are slightly weaker than in the reanalysis. During JJA, the large inter-seasonal changes associated with the Asian summer monsoons are captured by GAMIL-L, although the westerlies over India are not as strong as in the reanalysis. Over the SH, during both DJF and JJA, the westerlies in GAMIL-L generally agree with the reanalysis, except with weaker intensities.

In the upper troposphere, GAMIL-L also produces an acceptable simulation (figure not shown here). During DJF, the strongest westerlies occur over the NH,

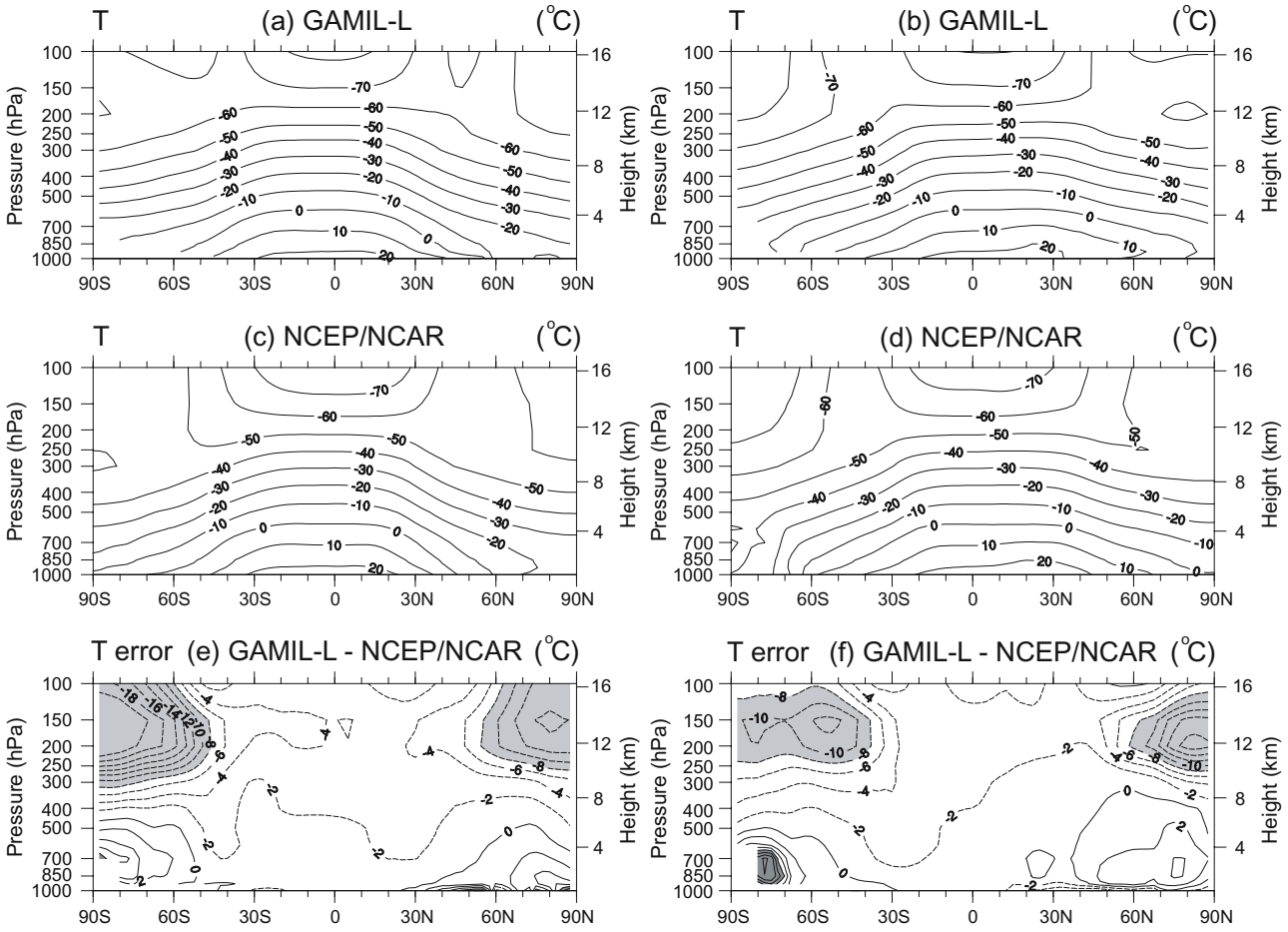

Fig. 8. Same as Fig. 1, but for mean zonally-averaged temperature (°C). The contour increment in the top two rows is 10°C. Differences are contoured every 2°C from 0°C.

and reach more than 60 m s^{-1} off the Asian coast and 40 m s^{-1} over eastern North America and the western Atlantic Ocean. Over the SH, the peak westerlies are reached between 40°–50°S with maxima over the Atlantic and Indian Oceans. All these features are in good agreement with the NCEP reanalysis. During JJA, the tropical easterlies over South Asia are well captured by GAMIL-L, and the strong Australia-New Zealand subtropical jet stream is also evident in the simulation.

Finally, the divergent wind and velocity potential at 200 hPa for GAMIL-L and the NCEP reanalysis are shown in Fig. 7. During both DJF and JJA, the structure of atmospheric transport of mass from the summer hemisphere to the winter hemisphere is well captured by GAMIL-L, suggesting an acceptable performance of the model in the upper troposphere. The major differences between the simulation and the reanalysis include a slightly stronger divergence over East Asia and a stronger convergence over the South Atlantic Ocean during JJA in the model.

3.4 *Temperature*

The tropospheric zonal mean temperature profile is shown in Fig. 8. In general, the temperature structures are reproduced by the model. During both DJF and JJA, the simulated upper troposphere temperature over the polar regions is colder, while in the lower troposphere it is hotter than in the reanalysis. This is one of the key reasons for the biases of geopotential height over high latitudes, as discussed above. On the other hand, simulated temperature over the tropics and mid latitudes are in reasonable agreement with the NCEP reanalysis.

Figure 9 shows that GAMIL-L overestimates the surface air temperature over the southern part of the Eurasia continent. During JJA, from Portugal to the Himalayas, GAMIL-L has a warm bias. Other small biases locate at Greenland, the Rocky Mountains, Australia and southern Africa, due to the model's coarse resolution over steep terrains.

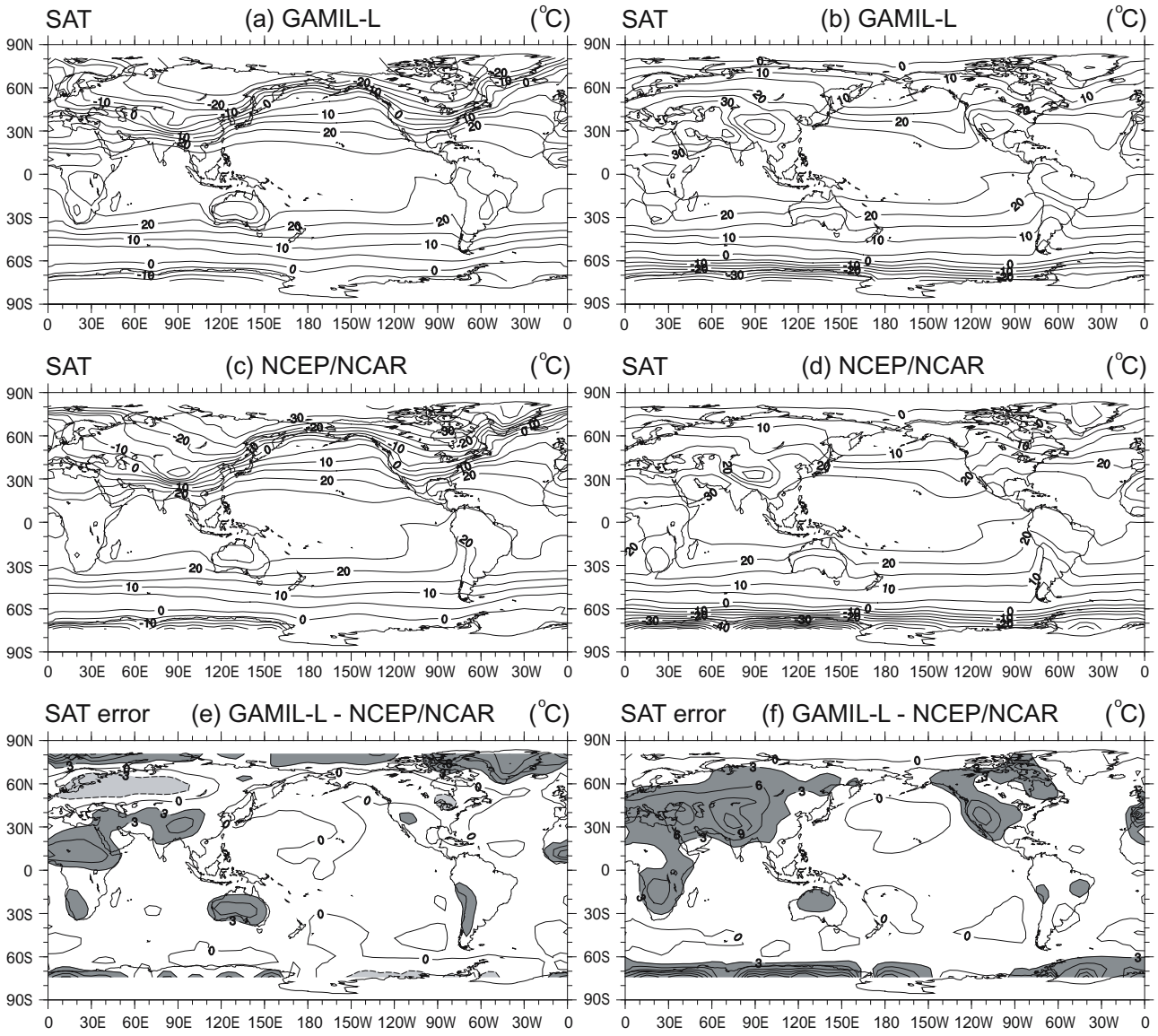

Fig. 9. Same as Fig.1, but for mean surface air temperature (°C). The contour increment in the top two rows is 5°C. Differences are contoured every 3° from 0°C.

3.5 *Precipitation*

Figure 10 compares the zonally-averaged rainfall simulated by GAMIL-L and from the CPC Merged Analysis of Precipitation (CMAP) (Xie and Arkin, 1996). The major model biaseslocate in the tropics, especially over the ITCZ of the summer hemisphere. During JJA, the maximum tropical precipitation in GAMIL-L is around 5 mm d^{-1} near 10°N, which is 4 mm d^{-1} less than in the CMAP data. Similarly, during DJF, the maximum in GAMIL-L is 2 mm d^{-1} less than for CMAP. This infers that the simulation of Hadley circulation in GAMIL-L is weaker than in the reanalysis. On the other hand, the subtropical rainfall minima are reproduced by GAMIL-L, although they are lower in the summer hemisphere and higher in the winter hemisphere. Finally, during both DJF and JJA, the simulated precipitation rates are slightly higher than the observational estimates over the mid to high latitudes.

Figure 11 shows that, during DJF, high rainfall rates associated with convection in the South Pacific and South Atlantic convergence zones are reasonably captured by GAMIL-L, but with a smaller area extent and a weaker magnitude. During JJA, the observed three maximum rainfall centers in the Bay of Bengal, the western North Pacific and the eastern Pacific, are generally captured by GAMIL-L. However,

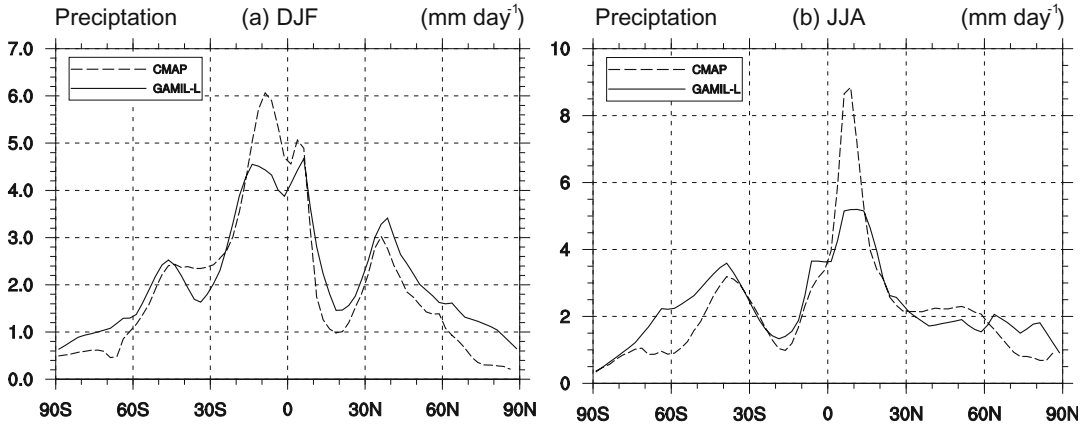

Fig. 10. Mean zonally-averaged precipitation (mm d^{-1}) for DJF (left) and JJA (right) from the model (solid line) and the NCEP/NCAR reanalysis (dashed line).

because of the weakly simulated Pacific ITCZ, the dumb-bell shape of the precipitation pattern is not evident in GAMIL-L. The bias in simulating the Indian monsoon rainfall is a chronic problem for the NCAR CCM family (Kang et al., 2002; Collins et al., 2003). With GAMIL-L using the physical package of CAM2, this simulated deficiency is not surprising. In addition, GAMIL-L simulates well the large-scale precipitations from mid latitudes to high latitudes during the winter hemisphere associated with fronts and cyclones.

Further examination revealed an erroneous precipitation center on the eastern periphery of the Tibetan Plateau. Similar bias has been reported in the CCM3 model (Yu et al., 2000). Simulation of the eastern Chinese climate remains a difficult task for the climate modelling community, and barely any model could realistically reproduce the mei-yu band (Kang et al., 2002; Zhou and Li, 2002). Like many other AGCMs, GAMIL-L also fails in reproducing the summer rainfall pattern over East Asia. The reason is attributed to an overestimated western Pacific subtropical high (WPSH). The western edge of the WPSH in GAMIL-L extends too far westward, reaching the eastern part of the Tibet Plateau. This transports too much moisture into eastern and central China, resulting in too much convective precipitation over the east of Tibet.

3.6 *Tropical inter-annual variability*

From the above analyses, it is evident that the tropical mean atmospheric circulation is generally captured by GAMIL-L. Over the tropics, there is a fairly direct tropospheric response to SST anomalies, which have a large inter-annual signal associated with ENSO. Here, we examine tropical atmospheric variability associated with ENSO, using the southern oscillation index (SOI) and the Indian summer monsoon index as two indicators.

We performed an EOF analysis of the monthly SLP fields from the simulation forced by observational SST between 1945–2000. The leading EOFs are presented in Fig. 12. The SLP pattern in the reanalysis is characterized by an anomalous sea-saw oscillation of SLP between the eastern Pacific and Indian Oceans. GAMIL-L reasonably captures this broad pattern, but with a slight shift to the east by around 30°. In the SST forced run, this model reproduces the SOI very well from 1950–2000 (Fig. 13), with a correlation coefficient of 0.92 with the reanalysis SOI.

Another important inter-annual signal in the tropics that can influence the East Asian climate is the Indian summer monsoon (ISM). Using Webster and Yang's definition of the South Asia dynamic monsoon index (Webster and Yang, 1992), the simulated inter-annual variability of the ISM in GAMIL-L was analyzed. As shown in Fig. 14, the simulated Webster-Yang Index (WYI) (Webster and Yang, 1992) time series is in good agreement with the reanalysis, with a correlation coefficient of 0.72.

Based on the above analysis, it is noted that GAMIL-L performs well in the tropics, not only for those primary fields of the meteorological variables, but also for some specific issues, such as atmospheric oscillation and monsoon system. Thus, if GAMIL-L is used as the atmosphere component of a coupled climate system model to simulate the paleoclimate, maybe some specific issues, such as ENSO and the Asian summer monsoon, will be the priorities.

4. Changes to GAMIL

4.1 *Zonal mean circulation*

The original version of GAMIL uses a 128×60 weighted equal-area mesh, which corresponds to an approximate $2.8° \times 2.8°$ grid, while GAMIL-L merely

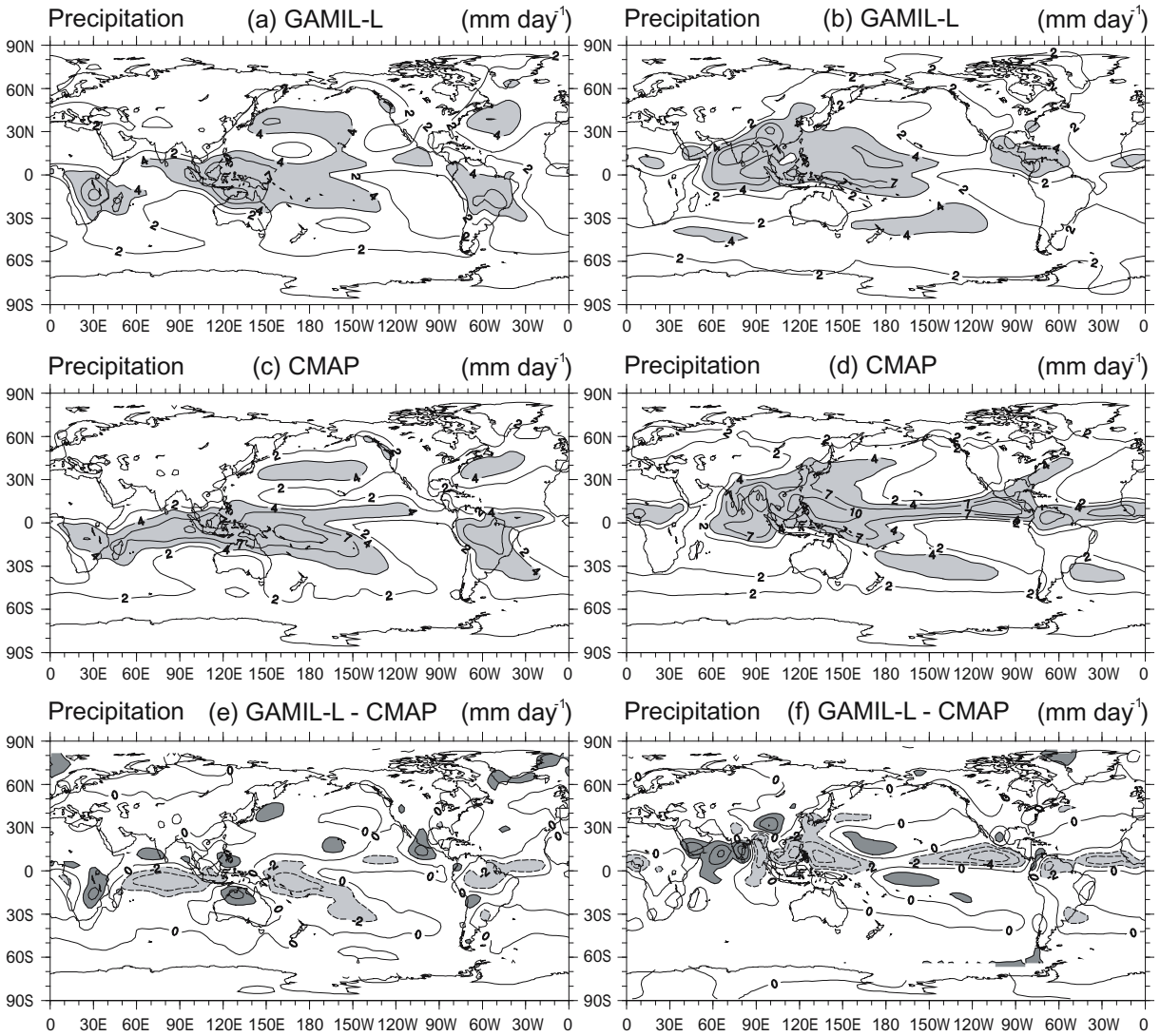

Fig. 11. Same as Fig. 1, but for mean total precipitation (mm d^{-1}). The contour in the top two rows is plotted in nonlinear levels (0, 2, 4, 7, 10, 15, 20, 25, 30 mm d^{-1}), and the values greater than 4 mm d^{-1} are shaded in light gray. Differences are contoured in nonlinear levels (± 2, ± 4, ± 7, ± 10 mm d^{-1}) from 0 mm d^{-1}.

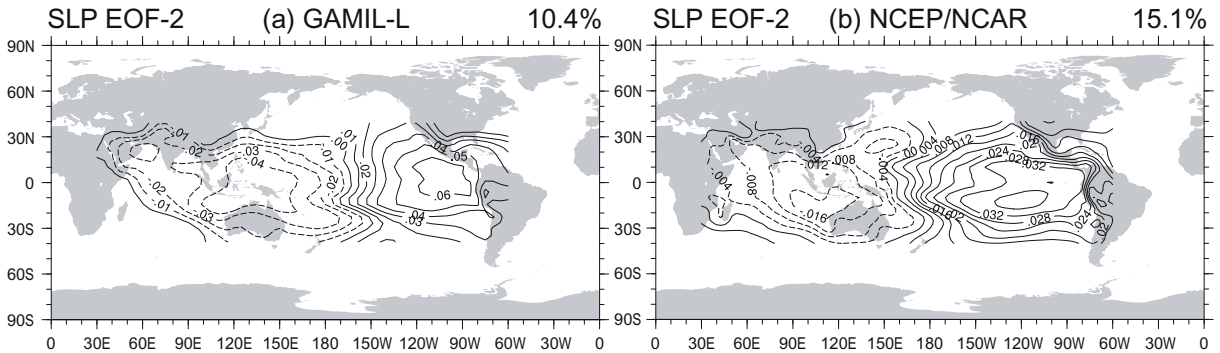

Fig. 12. The second leading EOF of monthly SLP from (a) the model and (b) the NCEP/NCAR reanalysis during 1951–2000. The model data is derived from the observational SST forcing run. This pattern corresponds to a positive phase in the SO and cold phase of El Niño.

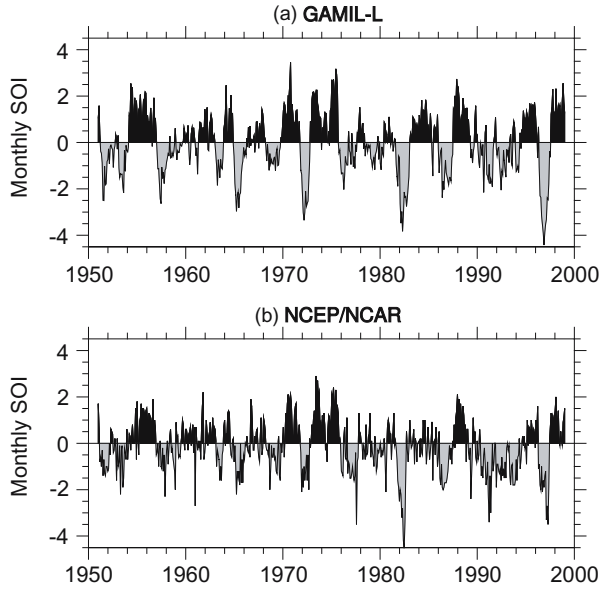

Fig. 13. Monthly SOI from (a) the model and (b) the NCEP/NCAR reanalysis from 1951–2000. The positive (negative) phases of SO are shaded in dark gray (light gray).

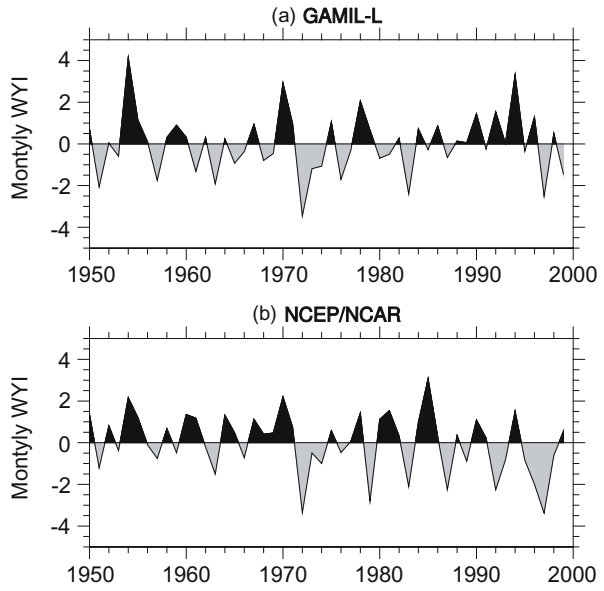

Fig. 14. Same as Fig.13, but for monthly Webster-Yang Index (WYI) (Webster et al., 1992) for South Asia summer monsoon.

uses a 72×40 mesh. Thus, it is noted that there are various differences in the simulated climatology between them. Particularly, GAMIL-L notably differs from GAMIL in polar regions due to its coarse resolution there. Therefore, the differences between these two models, especially over polar regions, are briefly investigated in this section.

Figure 15 shows the differences in geopotential height, temperature and zonal wind between the low and high resolution versions of GAMIL. It is evident that the major biases generally locate in the high latitudes and polar regions. In the NH, the middle and upper troposphere at high latitudes in GAMIL-L suffer cooler and higher conditions than those in the original version of GAMIL for both DJF and JJA, suggesting a stronger boreal polar vortex simulated by GAMIL-L, especially in the NH summer. In the SH, due to the coarse expression of terrain in a low resolution grid, the mean altitude of Antarctica in GAMIL-L is evidently lower than that in GAMIL, resulting in a anomalous warm center and a positive height center around this continent from the lower to middle troposphere for DJF and JJA. In the upper troposphere, there are two negative centers of geopotential height, one of which shifts from 45°S in DJF to 30°S in JJA, inducing the strongest gradient from the polar region in the lower level to mid latitudes in the upper level. Thus, one steady eastern wind anomaly always maintains from 40°–60°S throughout a year, suggesting a weak western wind zone in mid latitudes of the SH in GAMIL-L, which is also identical with the analysis of zonal wind in section 3.3. The polar vortex of the SH in GAMIL-L is overestimated, accompanying a stronger western wind from 80°–90°S.

From the above discussion, it is easy to establish that the biases between GAMIL-L and GAMIL versions are generally situated in the higher latitudes, especially in two polar regions, rather than in the tropics and the mid latitudes. On the other hand, the biases in the SH are larger than those in the NH due to the coarse representation of steep terrain over Antarctica in GAMIL-L.

4.2 *Polar regions*

Because the major biases centralize in the polar regions, we take the north polar region as an example to examine the circulation features in this section. Figure 16 shows the difference between GAMIL-L and GAMIL in the fields of SLP, 850 hPa wind and 500 hPa geopotential height. During DJF, the polar vortex in GAMIL-L is stronger than that in GAMIL, which is consistent with the above arguments. Simultaneously, the two continents, Eurasia and North America, are both covered by the overestimated high SLP, while the two oceans (the North Pacific and North Atlantic) are covered by the underestimated SLP. The corresponding fields of 850 hPa wind and 500 hPa geopotential height are presented in Figs. 16c and 16e. It is easy to establish that the major differences correspond to the coastlines, especially the zero contour line, which is obviously distinguishable along the edge of the lands. This means that most biases between GAMIL-L and

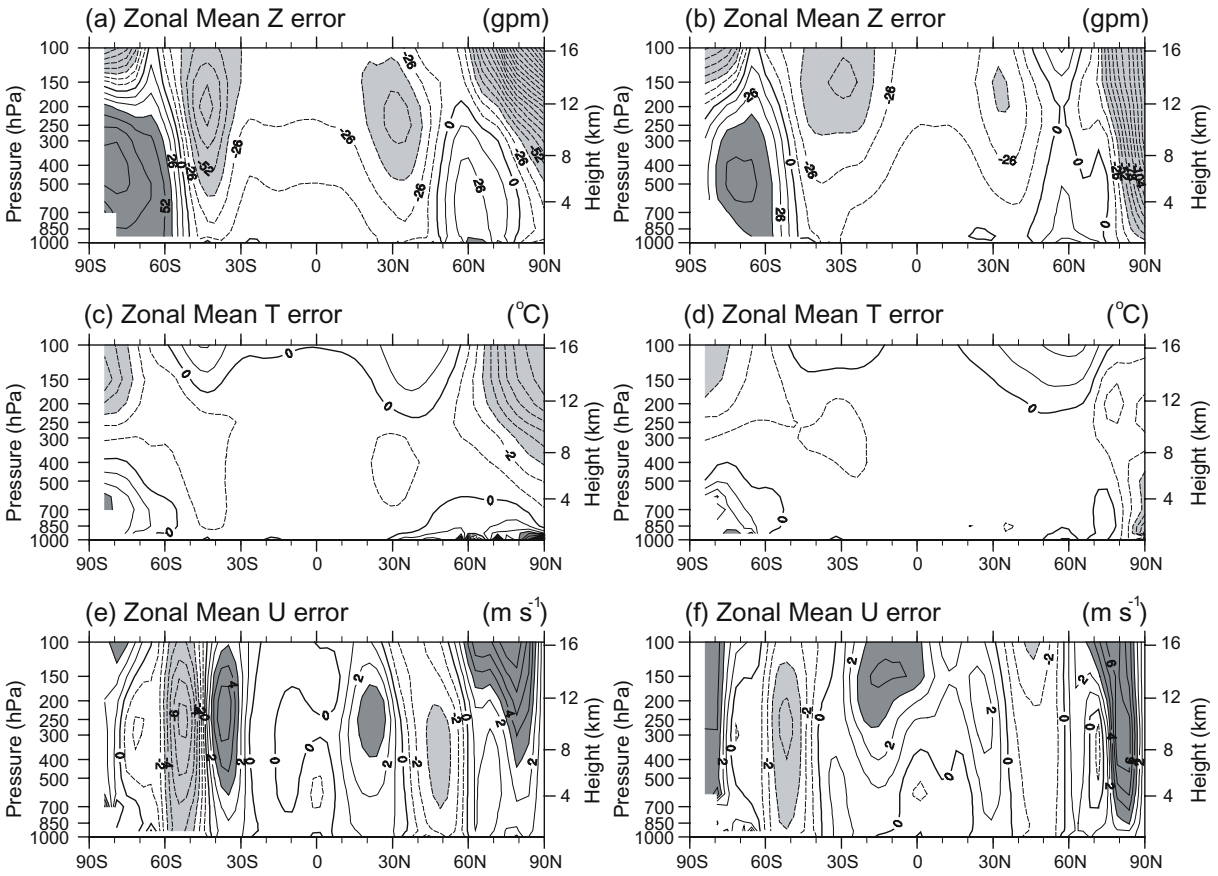

Fig. 15. Long-term mean differences of zonally-averaged geopotential height (top row, units: gpm), temperature (middle row, units: °C) and zonal wind (bottom row, units: m s^{-1}) between GAMIL-L and GAMIL for DJF (left) and JJA (right). The contour increments are 13 gpm (top), 1°C (middle) and 1 m s^{-1} (bottom) separately. Positive (negative) differences that are statistically significant at the 95% level for a t-test are shaded in dark gray (light gray).

GAMIL can be attributed to the different representation of the terrains via their various resolution grids. During JJA, almost the same conclusion can be drawn.

More comparisons show that the differences between GAMIL-L and GAMIL are mostly caused by the grid size in all seasons. In the polar regions, neither GAMIL-L nor GAMIL reproduce the realistic climatology, though GAMIL performs slightly better.

5. Summary

A fast integration version of the Grid Atmosphere Model of IAP/LASG, namely GAMIL-L, is developed. This study provides an assessment of climatological mean states of GAMIL-L. Regarding dynamical aspects, such as SLP, geopotential height and wind fields; and thermodynamic aspects, such as precipitation and temperature, we have shown that GAMIL-L can capture most large-scale features seen in the NCEP/NCAR reanalysis and the CMAP data. The simulated dynamical features are in reasonable agreement with the reanalysis at low and mid latitudes, where the thermodynamic features show corresponding biases, especially in precipitation fields. Due to the coarse resolution of the model over polar regions, both the dynamical and thermodynamic features are not well simulated by GAMIL-L in these areas. When forced by observational monthly SST, the model produces a fairly realistic simulation of the inter-annual variability associated with the Southern Oscillation and the Indian summer monsoon, suggesting that the model is suitable for climate modeling over either the tropics or the mid latitudes.

GAMIL-L retains most of the features compared with the original version, especially in the tropics and mid latitudes, although it is only a very low resolution model. In the high latitudes and polar regions, their differences evidently accord with the edge between land and sea. Because their differences in the representations of the terrain due to the various grids in the tropics and mid latitudes are not as distinct as those in the high latitudes and polar regions, the bi-

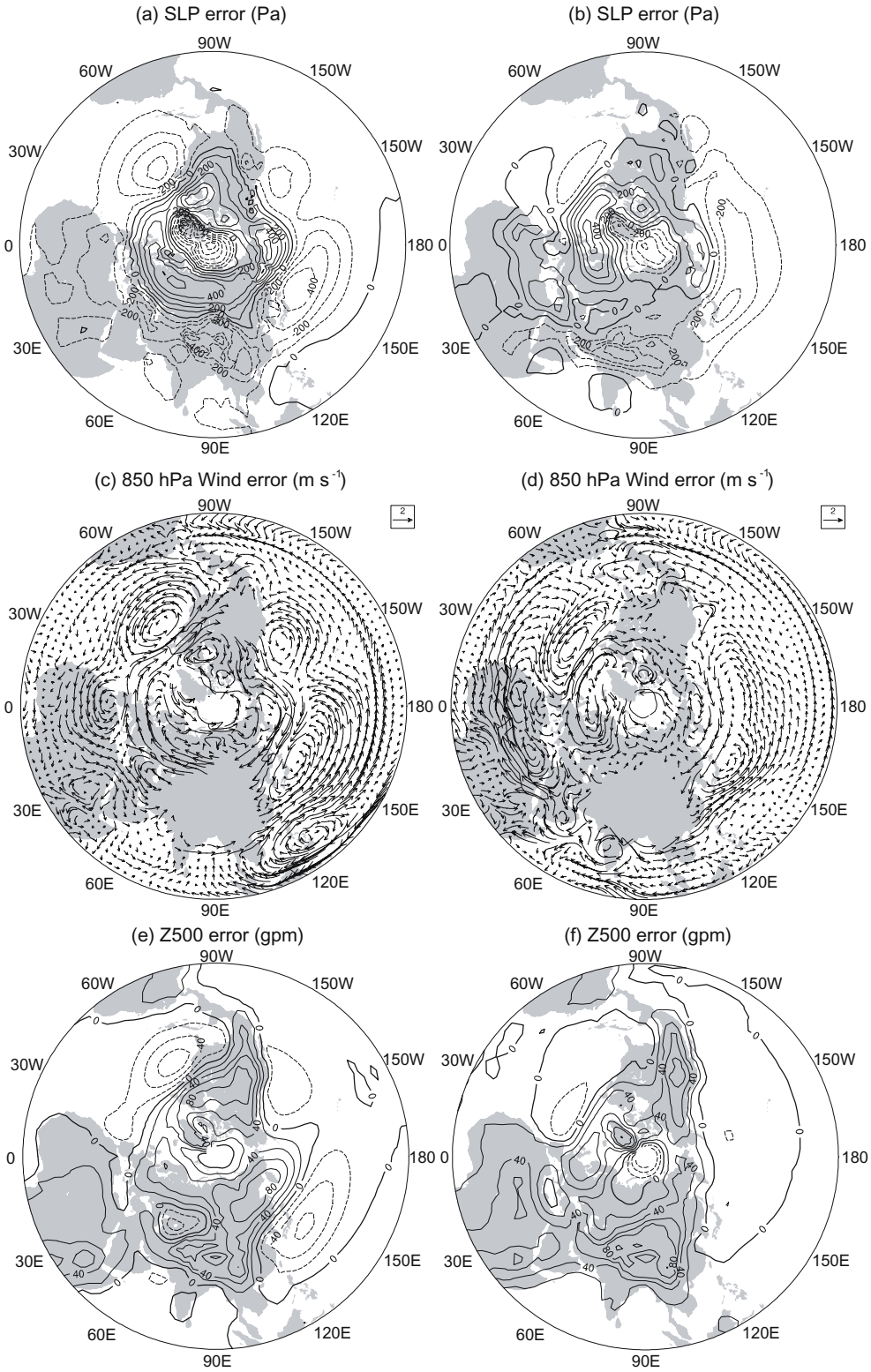

Fig. 16. Long-term mean differences of SLP (top row), 850 hPa wind (middle row) and 500 hPa geopotetial height (bottom row) between GAMIL-L and GAMIL for DJF (left) and JJA (right). The contour increments are 100 Pa (top) and 40 gpm (bottom) separately.

ases between the low and high resolution models can be attributed to the grid size.

In addition, because of its high computational efficiency, we have employed GAMIL-L as the atmospheric component of a fully coupled climate system model, for fast integrations in paleoclimate studies. Up to now, more than 1000 years of coupled integration have been completed. Details of this coupled model and more analyses will be presented in a separate paper.

Acknowledgements. This work was jointly supported by the Chinese Academy of Sciences under the project of the International Partnership Creative Group "The Climate System Model Development and Application Studies" and the Major State Basic Research Development Program of China under Grant No. 2005CB321703. This work also contributes to the LASG/IAP Short-term Visiting Scholar program. The model integration was performed on the "Lenovo DeepComp 6800" supercomputer at the Supercomputing Center of the Chinese Academy of Sciences.

REFERENCES

Bao, Q., Y. Liu, T. Zhou, Z. Wang, G. Wu, and P. Wang, 2005: The Sensitivity of the New Atmospheric General Circulation Model SAMIL-R42L26 of LASG/IAP to the land-atmosphere flux. *Chinese J. Atmos. Sci.*, **30**(6), 1077–1090.

Blackmon, M., and Coauthors, 2001: The community climate system model. *Bull. Amer. Meteor. Soc.*, **82**, 2357–2376.

Boville, B. A., and P. R. Gent, 1998: The NCAR Climate System Model, version one. *J. Climate*, **11**, 1307–1326.

Climate and Global Dyamics Division, 2004: Annual Scientific Report 2004: Community Climate System Model Narrative. [available online at http://www.cgd.ucar.edu/asr/asr04/ccsm/ narrative_ccsm.html].

Collins, W. D., and Coauthors, 2003: Description of the NCAR Community Atmosphere Model (CAM2). National Center for Atmospheric Research, Boulder, Colorado, 171pp.

Dixon, K. W., T. L. Delworth, T. R. Knutson, M. J. Spelman, and R. J. Stouffer, 2003: A comparison of climate change simulations produced by two GFDL coupled climate models. *Global and Planetary Change*, **37**, 81–102.

Hack, J. J., J. T. Kiehl, and J. W. Hurrell, 1998: The hydrologic and thermodynamic characteristics of the NCAR CCM3. *J. Climate*, **11**, 1179–1206.

Hurrell, J. W., J. J. Hack, B. A. Boville, D. L. Williamson, and J. T. Kiehl, 1998: The dynamical simulation of the NCAR Community Climate Model version 3 (CCM3). *J. Climate*, **11**, 1207–1236.

Jacob, R., C. Schafer, I. Foster, M. Tobis, and J. Anderson, 2001: Computational design and performance of the Fast Ocean Atmosphere Model. Proc. 2001 International Conference on Computational Science, Alexandrov et al. Eds., Springer-Verlag, 175–184.

Jones, C., J. Gregory, R. Thorpe, P. Cox, J. Murphy, D. Sexton, and P. Valdes, 2005: Systematic optimization and climate simulation of FAMOUS, a fast version of HadCM3. *Climate Dyn.*, **25**, 189–204.

Kalnay, E., and Coauthors, 1996: The NCEP/NCAR 40-year reanalysis project. *Bull. Amer. Meteor. Soc.*, **77**, 437–471.

Kang, I.-S., and Coauthors, 2002: Intercomparison of the climatological variations of Asian summer monsoon precipitation simulated by 10 GCMs. *Climate Dyn.*, **19**, 383–395.

Kiehl, J. T., J. J. Hack, G. B. Bonan, B. A. Boville, D. L. Williamson, and P. J. Rasch, 1998a: The National Center for Atmospheric Research Community Climate Model: CCM3. *J. Climate*, **11**, 1131–1149.

Kiehl, J. T., J. J. Hack, and J. W. Hurrell, 1998b: The energy budget of the NCAR Community Climate Model: CCM3. *J. Climate*, **11**, 1151–1178.

Liu, Z., W. Lewis, and A. Ganopolski, 2004: An acceleration scheme for the simulation of long-term climate evolution. *Climate Dyn.*, **22**, 771–781.

Raphael, M. N., 1998: Quasi-stationary waves in the Southern Hemisphere: An examination of their simulation by the NCAR Climate System Model, with and without an interactive ocean. *J. Climate*, **11**, 1405–1418.

Rayner, N. A., D. E. Parker, E. B. Horton, C. K. Folland, L. V. Alexander, D. P. Rowell, E. C. Kent, and A. Kaplan, 2003: Global analyses of SST, sea ice and night marine air temperature since the late nineteenth century. *J. Geophys. Res.*, **108**(D14), 4407, doi:10.1029/2002JD002670.

Russell, G. L., J. R. Miller, and D. Rind, 1995: A coupled atmosphere-ocean model for transient climate change studies. *Atmos.-Ocean*, **33**, 683–730.

Tobis, M., C. Schafer, I. Foster, R. Jacob, and J. Anderson, 1997: FOAM: Expanding the horizons of climate modeling. Proc., Super Computing 1997, San Diego, California, ACM/IEEE, pp27.

Wang, B., H. Wan, Z. Ji, X. Zhang, R. Yu, Y. Yu, and H. Liu, 2004: Design of a new dynamical core for global atmospheric models based on some efficient numerical methods. *Science in China, Ser. A*, **47**, 4–21.

Webster, P. J., and S. Yang, 1992: Monsoon and ENSO: selectively interactive systems. *Quart. J. Roy. Meteor. Soc.*, **118**, 877–926.

Wu, G., H. Liu, Y. Zhao, and W. Li, 1996: A nine-layer atmospheric general circulation model and its performance. *Adv. Atmos. Sci.*, **13**, 1–18.

Wu, T., P. Liu, Z. Wang, Y. Liu, R. Yu, and G. Wu, 2003: The performance of atmospheric component model R42L9 of GOALS/LASG. *Adv. Atmos. Sci.*, **20**, 726–742.

Xie, P. P., and P. A. Arkin, 1996: Analyses of

global monthly precipitation using gauge observations, satellite estimates, and numerical model predictions. *J. Climate*, **9**, 840–858.

Yu, R., W. Li, X. Zhang, Y. Yu, H. Liu, and T. Zhou, 2000: Climatic features related to eastern China summer rainfalls in the NCAR CCM3. *Adv. Atmos. Sci.*, **17**, 503–518.

Zeng, Q. C., C. G. Yuan, X. H. Zhang, X. Z. Liang, and N. Bao, 1987: A global grid point general circulation model. Collection of papers presented at the WMO/IUGG NWP Symposium, Tokyo, 4–8 Aug. 1986. *J. Meteor. Soc. Japan*, Special Volume, 121–124.

Zhang, X., N. Bao, R. Yu, and W. Wang, 1992: Coupling scheme experiments based on an atmospheric and oceanic GCM. *Chinese J. Atmos. Sci.*, **16**(2), 129–144.

Zhou, T. J., and Z. X. Li, 2002: Simulation of the East Asian summer monsoon by using a variable resolution atmospheric GCM. *Climate Dyn.*, **19**, 167–180.